ISSN 0915-633X

NATIONAL INSTITUTE FOR FUSION SCIENCE

Interactions of Convecting Magnetic Loops and Arcades

M. Ozaki, T. Sato and the Complexity Simulation Group

(Received - Aug. 7, 1996)

NIFS-448 Sep. 1996

RESEARCH REPORT
NIFS Series

NAGOYA, JAPAN

INTERACTIONS OF CONVECTING MAGNETIC LOOPS AND ARCADES

MASAO OZAKI[a], TETSUYA SATO, and the Complexity Simulation Group[b]

Theory and Computer Simulation Center, National Institute for Fusion Science, Nagoya 464-01, Japan

Interactions of magnetic loops and arcades that are convecting at their photospheric footpoints are investigated by means of a three-dimensional magnetohydrodynamic simulation. The initial magnetic field is given by solving the bipolar potential field emerging from paired conevection holes on the photospheric plane under which magnetic fluxes are supplied. Simulations are performed for single bipolar flux tubes and twin bipolar flux tubes with loop-like and arcade-like shapes. It is found that a prominent energy release can occur only when two flux tubes collide and reconnect with each other. The releasing feature becomes more intensive and narrowly peaked as resistivity becomes smaller, which reflects a nature of driven reconnection. A single loop or arcade does not exhibit any significant energy release, even though it is highly twisted and expanded.

[a] On leave from Institute of Industrial Science, University of Tokyo

[b] T. Hayashi, R. Horiuchi, K. Watanabe, Y. Todo, A. Kageyama, T. H. Watanabe, and H. Takamaru.

KEYWORDS: solar flare, coronal magnetic field, magnetic reconnection

1. INTRODUCTION

Self-organization is a generic concept common to many attractive dynamic phenomena which exhibit ordered behaviors in complex systems (Sato 1996). In a magnetohydrodynamic (MHD) plasma, it is well known that a well-organized magnetic field structure is formed as a result of a kink instability whereby free magnetic energy is released to kinetic and thermal energies in a fast time scale (Horiuchi & Sato 1985). Since the time scale of the normal resistive diffusion, caused by particle collisions, in a high-temperature rarefied plasma such as the coronal plasma is much larger than the MHD time scale, the mechanism of explosive energy release cannot be attributed to the simple resistive diffusion. The most likely mechanism resposible for the rapid energy release is the driven magnetic reconnection process (Sato & Hayashi 1979). The energy source of the solar flare, i.e., the explosive energy release in a coronal magnetized plasma, is commonly believed to be the magnetic field and the primary way of accomplishing its release is magnetic reconnection (Priest 1982). Therefore, it is meaningful to study the solar flare as a typical self-organization phenomenon associated with magnetic reconnection.

Developments of radio and X-ray astronomy have revealed that the solar corona is a high-temperature ($\sim 10^6$ K) rarefied plasma highly-related with a magnetic loop/arcade over sunspots. It is usually accepted that a sunspot results from magnetic buoyancy acting on a solitary magnetic flux tube which is generated by the dynamo action in the solar convective zone (Parker 1955). The solar flare is generally considered to result from energy release of twisted or sheared

magnetic fields (Kurokawa 1988). The coronal magnetic field lines are anchored at the photosphere. Subphotospheric convection, which is induced by heat transfer in the convection zone, can twist coronal magnetic field lines. Since the inertia of the photospheric plasma is much larger than that of the coronal plasma, the photospheric flows drag the coronal field lines. This implies that the coronal magnetic field lines strongly suffer from deformation due to photospheric flows, hence, the photospheric convection is very likely to be a primary energy activation source of various phenomena in the coronal region.

It is known that magnetic flux tubes become unstable to kink modes if they become sufficiently twisted. In a magnetically confined fusion plasma device such as the pinch and tokamak discharges, MHD kink modes become destabilized if the plasma current, which is proportional to the twist of the field, exceeds a threshold value, the Kruskal-Shaflanov limit (Kruskal et al. 1958; Shafranov 1958). Although many authors have studied the stability of twisted magnetic flux tubes which are "line-tying" at the ends of the tubes, they have modelled a coronal magnetic loop as a straight geometry (Einaudi & Van Hoven 1983; Craig & Sneyd 1990; Foote & Craig 1990; Mickić, Schnack, & Van Hoven 1990; Velli, Einaudi, & Hood 1990). Besides the study on the three dimensional force-free MHD equibrium of the twisted flux tubes (Finn, Guzdar, & Usikov 1994), evolution of coronal magnetic fields caused by footpoint motions have been studied by many authors (Biskamp & Welter 1989; Wu, Song, & Martens 1991; Rickard & Priest 1994; Wang & Bhattacharjee 1994; Mikić, Barnes, & Schnack 1988; Mikić 1990). However, some of them are two-dimensional studies, which are models of

coronal arcades (Biskamp & Welter 1989; Wu et al. 1991; Rickard & Priest 1994; Wang & Bhattacharjee 1994); the others are done under the periodic boundary condition, where magnetic reconnection can take place artificially at the boundary (Mikić et al. 1988; Mikić 1990).

Recently, Kusano et al. (1994) have studied the detailed energy relaxation process of twisted flux tubes by means of a three-dimensional MHD simulation, paying particular attention to the relationship with the Taylor hypothesis (Taylor 1974, 1986). They, however, assumed a peridoc boundary condition which stimulates artificial reconnection at the boundary. In this respect, Van Hoven, Mok, and Mikić (1995) executed a three dimensional MHD simulation, in which the magnetic field is not straight and the periodic boundary condition is not adopted. However, their results were a bit premature to provide sufficient information on solar flare phenomena. In contrast, a recent work of Amo et al. (1995) has shown an interesting intermittent behavior in energy release and topological change for a continuously twisted straight magnetic flux tube surrounded by untwisted uniform field lines.

In this paper we wish to investigate a three-dimensional dynamical evolution of twisted magnetic flux loops and sheared arcades without invoking a periodic boundary condition which allows an involvement of infinite energy, but with a more realistic geometrical condition where the magnetic flux is supplied from isolated photospheric regions.

In section 2 we describe the present simulation model. In section 3 the evolution of magnetic fields is studied for a single convecting magnetic loop and arcade.

In section 4 the interaction of paired convecting magnetic loops and arcades is studied. Conclusion is given in section 5.

2. SIMULATION MODEL

The basic equations to be solved are the incompressible, dissipative MHD equations:

$$\rho \frac{d\boldsymbol{v}}{dt} = \boldsymbol{J} \times \boldsymbol{B} + \nu \nabla^2 \boldsymbol{v}, \tag{1}$$

$$\frac{\partial \boldsymbol{B}}{\partial t} = -\mathrm{rot}\boldsymbol{E} \tag{2}$$

$$\mu_0 \boldsymbol{J} = \mathrm{rot}\boldsymbol{B}, \tag{3}$$

$$\boldsymbol{E} = -\boldsymbol{v} \times \boldsymbol{B} + \eta \boldsymbol{J}, \tag{4}$$

where ρ is the mass density, $\boldsymbol{v}$ is the flow velocity, $\boldsymbol{B}$ is the magnetic field, $\boldsymbol{J}$ is the electric current density, $\boldsymbol{E}$ is the electric field, η is the electrical resistivity, ν is the coefficient of viscosity, and μ_0 is the magnetic permeability in vacuum.

We assume that the mass density ρ is constant ρ_0. The thermal energy converted from the magnetic and flow energies is assumed to be immediately released outside by radiation or some other processes.

We use a three-dimensional Cartesian coordinate system. The simulation domain is given by a rectangular box which is bounded by the perfectly conducting walls located at $x = \pm L_x/2$, $y = \pm L_y/2$, and $z = 0, L_z$.

The evolutions of the magnetic and kinetic energies in the system are described by the following equations which are derived from the equations (1)-(4),

$$\frac{\partial W_B}{\partial t} = P - V_1 - R \tag{5}$$

$$\frac{\partial W_K}{\partial t} = V_1 - V_2, \tag{6}$$

where

$$W_B = \int \frac{1}{2\mu_0} \boldsymbol{B}^2 dV, \tag{7}$$

$$W_K = \int \frac{1}{2}\rho_0 \boldsymbol{v}^2 dV, \tag{8}$$

$$P = -\frac{1}{\mu_0}\int \boldsymbol{E}\times\boldsymbol{B}\cdot d\boldsymbol{S}, \tag{9}$$

$$R = \int \eta \boldsymbol{J}^2 dV, \tag{10}$$

$$V_1 = \int \boldsymbol{J}\times\boldsymbol{B}\cdot\boldsymbol{v}dV, \tag{11}$$

$$V_2 = -\int \nu\boldsymbol{v}\cdot\nabla^2\boldsymbol{v}dV. \tag{12}$$

Here, W_B is the total magnetic energy, W_K is the total kinetic energy, P is the Poynting vector flux through the boundary, R is the resistive energy dissipation rate, V_1 is the conversion rate between the kinetic and magnetic energies, and V_2 is the viscous energy dissipation rate, The Poynting vector flux P represents the energy flow by the convection at the photospheric footpoint of the emerging magnetic field lines.

The initial magnetic field is a current-free (potential) bipolar field whose normal component at the photospheric base ($z = 0$) is specified. We perform simulations for two types of initial magnetic field configuration, namely, a bipolar configuration and a paired bipolar configuration. The shape of the footpoint convection hole from which magnetic flux is supplied is changed from round to elliptic as indicated in Fig. 1. The normal component of the magnetic field at the footpoint (base) is given by

$$\begin{aligned} B_z &= \pm B_0 \frac{\cos(\pi r_i)+1}{2} \quad && r_i \le 1, \\ &= 0 && r_i > 1, \end{aligned} \tag{13}$$

where $r_i = \sqrt{(x-x_{ci})^2/r_x^2 + (y-y_{ci})^2/r_y^2}$ which is a coordinate designating a concentric ellipse, the index i running from 1 to 2 or 4, depending on whether

the magnetic configuration is a single bipolar type or a paired bipolar type. The center of the positive ($B_z > 0$) or the negative ($B_z < 0$) polarity region is located at $(x_{ci}, y_{ci}, 0)$, and r_x and r_y designate the shape of the convection zone.

In a photospheric hole region we impose a plasma convection by which the footpoint of a magnetic field line is driven to circulate. The convection motion imposed at the base is derived by the stream function $\Psi(r_i)$ which is constant at the convection boundary,

$$\begin{aligned}
&\Psi(r_i) \\
&= -\frac{v_0}{8r_{10}} r_i^4 + \frac{3v_0}{4r_{10}} r_i^2 && r_i \le r_{10}, \\
&= \frac{v_0}{2h^3}(r_i - r_{10})^4 - \frac{v_0}{h^2}(r_i - r_{10})^3 + v_0(r_i - r_{10}) + \frac{5}{8} v_0 r_{10} && r_{10} < r_i \le r_{20}, \\
&= \frac{v_0}{2} h + \frac{5}{8} v_0 r_{10} && r_i > r_{20}, \qquad (14)
\end{aligned}$$

where $h = r_{20} - r_{10}$. The stream function is determined by satisfying the following condition for the circular (round) motion. Taking a cylindrical coordinate system (r, θ, z) around the center of rotation, the velocity at the base is expressed as,

$$\begin{aligned}
v_\theta(r) &= g(r) && r \le r_{10}, \\
&= h(r) && r_{10} < r \le r_{20}, \\
&= 0 && r > r_{20}, \qquad (15)
\end{aligned}$$

where $g(r)$ is a monotonically increasing polynomial of degree three which satisfies

$$g(0) = 0, \ \left.\frac{d(g(r)/r)}{dr}\right|_{r=0} = 0, \ g(r_{10}) = v_0, \ \left.\frac{dg(r)}{dr}\right|_{r=r_{10}} = 0, \qquad (16)$$

and $h(r)$ is a monotonically decreasing polynomial of degree three which satisfies

$$h(r_{10}) = v_0, \ \left.\frac{dh(r)}{dr}\right|_{r=r_{10}} = 0, \ h(r_{20}) = 0, \ \left.\frac{dh(r)}{dr}\right|_{r=r_{20}} = 0. \qquad (17)$$

Note that v_0 is the maximum speed in the convection hole. The flow velocity at the base is then given by

$$v_x = -\frac{\partial \Psi}{\partial y} f(t), \tag{18}$$

$$v_y = \frac{\partial \Psi}{\partial x} f(t). \tag{19}$$

The function $f(t)$ is a smooth increasing function,

$$\begin{aligned} f(t) &= \frac{1 - \cos \frac{\pi t}{T_s}}{2} \qquad t < T_s, \\ &= 1 \qquad\qquad\qquad t \geq T_s, \end{aligned} \tag{20}$$

which is introduced to avoid a numerical artifact due to the sudden start of the rotation at $t = 0$. The convection motion of plasma naturally acts to induce a twisting or shearing of the magnetic field lines.

In the actual calculations all variables are normalized by the following three characteristic quantities and their combinations; the magnetic field B_0, Alfvén speed $V_A = B_0/\sqrt{\mu_0 \rho_0}$, and the length L. The time, the electric current, the electric field, the resistivity, and the viscosity coefficient are normalized by L/V_A, $B_0/\mu_0 L$, $V_A B_0$, $\mu_0 L V_A$, $\rho_0 L V_A$, respectively. The normalized energy U_0 is defined by B_0^2/μ_0. Hereafter we use the normalized quantities without noticing.

In the present study we consider three different configurations for the photospheric hole pair from which the bipolar magnetic flux emerges, as shown in Fig. 1. The choice is done to know the difference in the evolution depending on whether the shape of the flux tube is loop-like or arcade-like. Namely, run 1a corresponds to a loop-like flux tube and run 1c is an arcade-like one. Run 1b is an intermediate case. Run 1a, run 1b and run 1c correspond to single bipolar

flux tubes, while run 2a, run 2b and run 2c to paired bipolar flux tubes. The size parameters are given in Table 1. As for the size of the whole simulation box, the value of $L_x = L_y = L_z = 2$ is chosen after having carried out several test runs for different box sizes. Resultantly, we have found that the choice of $L_x = L_y = L_z = 2$ is large enough to dismiss the boundary effect. In other words, by choosing this size we have been able to conclude that the observed results are free from the presence of the artificial simulation boundary which cannot be avoided. The resistivity η and the viscosity coefficient ν are uniform and constant $\eta = 10^{-4}$ and $\nu = 10^{-3}$, unless otherwise specified.

We use the explicit method to solve the MHD equations numerically. The spatial derivative is approximated by the second order central difference scheme. The forward and backward differences are used to compute the derivative of fields at the boundaries.

The temporal integration is performed by the forth order Runge-Kutta-Gill method. The simulation domain ($L_x \times L_y \times L_z$) is devided into $101 \times 101 \times 101$ grids.

3. EVOLUTIONS OF SINGLE BIPOLAR LOOP AND ARCADE

We start with representing how a single bipolar flux tube behaves in response to three different convection motions of the footpoint, namely, run 1a (circular motion), run 1b (elliptic motion) and run 1c (highly elongated elliptic motion). Run 1a corresponds to a loop-like magnetic configuration, while run 1c to an arcade-like configuration. The parameters designating convection motions of these simulation runs are shown in Table 1(a).

The time development of the magnetic field lines for a bipolar flux loop (run 1a) is shown in Fig. 2. Plotted in this figure are twelve representative field lines which start from the points located on the left side circle (red) designated by $r_1 = 0.1$ and the right side one (green) designated by $r_2 = 0.1$. The square box drawn at the base does not represent the whole base domain, but a part of the base domain ($x = -0.5, 0.5$; $y = -0.5, 0.5$) of the whole simulation box ($x = -1, 1$; $y = -1, 1$; $z = 0, 2$).

As one sees in Fig. 2, at $t = 2\ \tau_A$, the representative magnetic field lines are only slightly twisted, but the kink distortion starts at about $t = 5\ \tau_A$ when the winding angle of the field line exceeds roughly 4.5π. We note here that the critical winding angle for the kink instability to be excited is 4.8π for the equilibrium with straight magnetic field configuration (Mickić et al. 1990). As time elapses, the twisted flux loop suffers a large kink distortion (see $t = 8\ \tau_A$). The loop expands vertically and horizontally about as three times large as the initial one because of the hoop ($\boldsymbol{J} \times \boldsymbol{B}$) force. At $t = 11\ \tau_A$, the loop has grown to a huge

size and the twirling of the magnetic field lines is distinctly seen. Nonetheless, no topological change in the magnetic field lines is observed. This indicates that no flare-like energy release due to reconnection has occurred.

Let us see what happens when the shape of the flux tube is different. Figure 3 shows the time development of the magnetic field lines for an arcade-like flux tube (runs 1c). The upper and lower panels are the magnetic field lines projected on the $x-y$ and $x-z$ planes, respectively. At $t = 17\ \tau_A$, the size of the arcade becomes about as nine times vertically and thirteen times horizontally large as the the initial one. At $t = 27\ \tau_A$ the arcade becomes huge but it appears that no distinct kink-like deformation has been seen as was observed in the previous run (run 1a, Fig. 2).

The evolution of magnetic field lines for the intermediate case (run 1b) is a little bit faster than that for the arcade-like case because of its relatively large shear motion, but the overall evolution is gentle and similar to that of run 1c.

Summarizing the results for runs 1a-1c, one can conclude that no drastic topological change of the magnetic field lines would occur in the case of single magnetic loop or arcade. This conclusion is in agreement with the results by Biskamp and Welter (1989) and Dahlburg, Antiochos, and Zang (1991). They have found that a single arcade remains stable while the footpoint is sheared. One new point we have obtained in the present study is that a kink-like twisted deformation takes place when the flux shape becomes more loop-like. It is said that an arcade-like structure is more gentle than a loop-like structure when the convection speed is the same.

4. EVOLUTIONS OF PAIRED BIPOLAR LOOPS AND ARCADES

Since it turns out that an isolated single loop or arcade does not exhibit any drastic energy release, we shall investigate evolutions of paired convecting magnetic loops and arcades. The central positions of the convection zones are located at $(x_{c1}, y_{c1}) = (-L_x/8, 0)$, $(x_{c2}, y_{c2}) = (-L_x/16, 0)$, $(x_{c3}, y_{c3}) = (L_x/16, 0)$, $(x_{c4}, y_{c4}) = (L_x/8, 0)$. The other parameters are shown in Table 1(b).

Figures 4 and 5 exhibit the time developments of the magnetic field lines for the loop-like and arcade-like cases (runs 2a and 2c, respectively) in the same format as Fig. 2. In these figures plotted are a pair of twelve representative field lines starting from the right hand side of the two pairs of convection ellipses designated by $r_2 = r_4 = 0.1$. As is seen in Fig. 4, in the early phase, e.g. at $t = 3\ \tau_A$, each loop evolves independently. At $t = 5\ \tau_A$ it is seen that each loop suffers a kink distortion in a similar way to that observed for the single loop (run 1a). Then, the distorted magnetic loops start reconnecting and the magnetic field lines originating from one loop are interchanged with those of the other loop. At $t = 7\ \tau_A$ magnetic reconnection is actively progressing and is completed at about $t = 8\ \tau_A$. The magnetic field line structure is drastically changed; a large outer loop overlies a small inner one. As time elapses, the larger outer loop keeps expanding vertically and horizontally (see $t = 15\ \tau_A$), while the smaller inner loop does not change much. During the evolution the reconnection region remains almost in the same place.

Let us move on to the arcade-like configuration. As is shown in Fig. 5, re-

connection starts between the two arcades at about $t = 5\ \tau_A$ and continues until about $t = 6.5\ \tau_A$. Then, the original parallel arcades are topologically changed into a pair of upper and lower arcades. As time elapses, the upper arcade expands vertically and horizontally while the smaller one remains almost the same. On comparing with the previous loop-like case, the overall behaviors are similar but the field line structure of the loop-like case becomes more complicated because of the superposition of kink-like deformation. This is because the twisting of a field line is larger for the loop-like case. The overall behavior for the intermediate case (run 2b) is similar to the other cases except that the field line twisting is in between.

Since an attractive force acts between the currents flowing along paired loops and arcades (Bhattacharjee, Brunel, & Tajima 1983; Longcope & Strauss 1994), reconnection has occured at the encounter point of them in the above cases. With intent to see what happens when a repulsive force works between two arcades, we have done another simulation run in which the direction of footpoint motion of the right hand side arcade is reversed (run 2c'). Figure 6 shows the time development of the magnetic field lines for this case. As the two arcades hoop, a repulsive force works between them. Thus, no global topological change of magnetic field lines has taken place. Grossly speaking, their behaviors look a superposition of two independent arcades (cf. Fig. 3).

In order to examine the dependence on the speed of footpoint motion, we have executed a run in which the speed is doubled (run 2c"). In this case reconnection starts at about $t = 3.5\ \tau_A$ and completes at about $t = 4.5\ \tau_A$. However, the

evolution pattern is very similar to run 2c where the speed was half of this case. Therefore, it can be said that as the footpoint speed becomes larger, the overall temporal evolution is hastened, but the evolution pattern is similar.

We also have performed a run (run 2c"') with $\eta = 10^{-3}$, in which the resistivity is as ten times large as that of run 2c with the other parameters the same. In this case reconnection starts at about $t = 6.5\tau_A$ and completes at about $t = 11.5\tau_A$. This result indicates that as the resistivity is increased in the resistivity range ($\eta = 10^{-4} \sim 10^{-3}$), the reconnection process becomes more diffusive and sloppy.

We shall see the plasma motion associated with reconnection. Figure 7 shows the plasma flow velocity on the $x-z$ plane at $t = 6\tau_A$ for run 2c. It is clearly seen that the overall flow consists of two patterns, i.e., hooping flow and reconnecting flow. The reconnecting flow, as a matter of course, is concentrated along the vertical axis ($x = 0$). More specifically, the attracting flows of two arcades, which are converging toward the central plane from the lower left- and the lower right-hand sides, collide at a reconnection point on the central plane and diverge out upwards and downwards. This flow pattern is a typical signature of the driven reconnection process. On the other hand, the hooping flow appears in the whole structure and acts to expand the (upper) arcade perpendicularly to its surface.

Figures 8(a) shows the temporal evolution of the heating rate (ohmic, viscous, and total heating) for run 2c in a local region bounded by $x = \pm 0.02$, $y = \pm 0.3$, and $0.057 \leq z \leq 0.37$. The region is chosen in such a way that the peaked current layer in the reconnection region can be sufficiently covered. The heating rate (Fig. 8(a)) has a sharp peak around $t = 7\ \tau_A$ when reconnection is actively

taking place. The maximum value of the total heating rate is about three times as large as that for run 2c' (Fig. 8(b)) where no reconnection takes place because of the repulsive force. This assures that when two flux loops or arcades collide and reconnection takes place, the magnetic energy is abruptly released into the plasma energy. The difference of the magnetic energy between these two cases may give us an estimate of the available energy for accelerating and/or heating the plasma. Thus, we have plotted the difference between the total magnetic energy for run 2c and that for run 2c' in Fig. 9 (a solid line), $\Delta W_{mag} = W_{mag,2c'} - W_{mag,2c}$, and also plotted its temporal rate (a dashed line), $\Delta(\Delta W_{mag})/\Delta t$. From $t \sim 5\tau_A$ to $t \sim 10\tau_A$, the energy difference rapidly increases. Especially noted is a sharp peak of $\Delta(\Delta W_{mag})/\Delta t$ at $t \sim 7.5\tau_A$, which is roughly consistent with the duration of active magnetic reconnection. The energy release rate is about $8 \times 10^{-4}\tau_A^{-1}$.

In order to see the role of resistivity on the evolution, we have done a simulation run in which the resistivity is changed. The heating rate for the case where the resistivity is increased from 10^{-4} to 10^{-3} (run 2c"') is shown in Fig. 10(b). The peak is not so sharp as that for run 2c where the resistivity is 10^{-4} (compare (a) and (b) of Fig. 10). The comparison of two cases gives us an important conclusion for the energy release due to the collision of two flux tubes, namely, that the energy release is more violent and squeezed as the resistivity becomes smaller. This conclusion is favorable for solar flares because the resistivity is so small. This important feature of inverse proportionality to resistivity can be easily explained by the driven reconnection process (Sato & Hayashi 1979; Sato, Horiuchi, & Kusano 1989). The hooping and attracting speed of the two arcades

(loops) may well be assumed to be the same for both cases. Then, the current at the encounter layer may roughly be given by

$$E_0 = \eta J \tag{21}$$

where E_0/B is the equivalent hooping/attracting speed (B is the representative magnetic field of the arcades which is reasonably assumed to be the same for both cases), which is considered to be the same for both cases. Thus, the current intensity is inversely proportional to the resistivity. The heating rate is proportional to ηJ^2, hence, J. Thus the heating rate is inversely proportinal to resistivity. In other words, the energy release occurs more violently as the resistivity becomes smaller. In the central solar corona the resistivity is quite small, so that it is expected that when two coronal magnetic arcades collide, magnetic energy can be released impulsively and intensively.

5. CONCLUSION

We have studied temporal evolutions of isolated covecting magnetic loops and arcades by a three-dimensional MHD simulation. As the initial magnetic field, a current-free (potential) bipolar field emerging from photospheric convection holes is given. Simulations are performed for a single bipolar flux tube and twin bipolar flux tubes.

In the case of a single magnetic loop or arcade, no drastic topological change of the magnetic field lines is observed. This result agrees with the previous ones (Biskamp & Welter 1989; Dahlburg et al. 1991). Namely, a single magnetic loop or arcade model may not be able to be a potential candidate for the topological change of magnetic field and the distinct energy release mechanism. In order to explain large energy release and drastic reconnection associated with a single magnetic loop or arcade, one may take overlying flux (ambient field) into account like an emerging flux model (Priest 1982; see also Amo et al. 1995). Specifically, a single twisting loop or shearing arcade can release magnetic energy only when the twisted field lines reconnect with ambient field lines.

In contrast, when two magnetic loops or arcades collide with each other, sailent magnetic reconnection is triggered because of the attractive force acting between the loop or arcade currents. Their evolution and resulting reconnection produce a larger overlying expanding loop (arcade) and a smaller lower one. Energy release becomes more intensive and impulsive as resistivity becomes smaller. These features can well be explained by driven reconnection and appear to be consistent with some important observational features of solar flares (converging

flux model: Priest, E. R., Parnell, C. E., & Martin, S. F. 1994; Parnell, C. E., Priest, E. R., & Golub, L. 1994).

ACKNOWLEDGMENTS

This work was supported by the Ministry of Education, Science and Culture Grants-in-Aid No. 07832024 and No. 08226104.

REFERENCES

Amo, H., Kageyama, A., Sato, T, & the Complexity Simulation Group 1995, Phys. Rev. E, 51, 3838

Bhattaccharjee, A., Brunel, F., & Tajima, T. 1983, Phys. Fluids, 26, 3332

Biskamp, D., & Welter, H. 1989, Solar Phys., 120, 49

Craig, J. D. & Sneyd, A. D. 1990, ApJ, 357, 653

Dahlburg, R. B., Antiochos, S. K., & Zang, T. A. 1991, ApJ, 383, 420

Einaudi, G., & Van Hoven, G. 1983, Solar Phys., 88, 163

Finn, J. M.,, Guzdar, P. N., & Usikov, D. 1994, ApJ, 427, 475

Foote, B. J., & Craig, I. J. D. 1990, ApJ, 350, 437

Horiuchi, R., & Sato, T. 1985, Phys. Rev. Lett., 55, 211

Kruskal, M. D., Johnson, J. L., Gottlieb, M. B., & Goldman, L. M. 1958, Phys. Fluids, 1, 421

Kurokawa, H. 1988, Space Sci. Rev., 51, 49

Kusano, K., Suzuki, Y., Kubo, H., Miyoshi, T., & Nishikawa, K. 1994, ApJ, 433, 361

Longcope, D. W., & Strauss, H. R. 1994, ApJ., 426, 742

Mikić, Z., Barnes, D. C., & Schnack, D. D. 1988, ApJ, 328, 830

Mikić, Z. 1990, Phys. Fluids, B2, 1450

Mikić, Z., Schnack, D. D., & Van Hoven, G. 1990, ApJ, 361, 690

Parker, E. N. 1955, ApJ, 122, 293

Parnell, C. E., Priest, E. R., & Golub, L. 1994, Solar Phys., 151, 57

Priest, E. R. 1982, Solar Magnetohydrodynamics (Dordrecht: Reidel)

Priest, E. R., Parnell, C. E., & Martin, S. F. 1994, ApJ, 427, 459

Rickard, G. J., & Priest, E. R. 1994, Solar Phys., 151, 107

Sato, T., Horiuch, R., & Kusano, K. 1989, Phys. Fluids, B1, 255

Sato, T., & Hayashi, H. 1979, Phys. Fluids, 22,1189

Sato, T. 1996, Phys. Plasmas, 3, 2135

Shafranov, V. D. 1958, Sov. Phys. JETP, 6, 545

Taylor, J. B. 1974, Phys. Rev. Lett., 33, 1139

Taylor, J. B. 1986, Rev. Mod. Phys., 58, 741

Van Hoven, G., Mok, Y., & Mikić, Z. 1995, ApJ, 440, L105

Velli, M., Einaudi, G., & Hood, A. W. 1990, ApJ, 350, 428

Wang, X., & Bhattacharjee, A. 1994, ApJ, 420, 415

Wu, S. T., Song, M. T., & Martens, P. C. 1991, Solar Phys., 134, 353

Figure Captions

Fig. 1: Six different shapes of the photospheric convection zones considered in this study. The upper panels represent the cases with a single magnetic flux tube and the lower the cases with a paired flux tube.

Fig. 2: Temporal evolution of the magnetic field lines for a single loop-like magnetic configuration (run 1a). The dashed lines at $t = 0$ designate the convection zone. The square box drawn at the base is a part of the base domain and not the whole base domain.

Fig. 3: Temporal evolution of the magnetic field lines for a single arcade-like magnetic configuration (run 1c). Upper panels show the projection on the $x - y$ plane (photospheric surface), and lower panels the projection on $x - z$ plane. The dashed lines at $t = 0$ designate the convection zone.

Fig. 4: Temporal evolution of the magnetic field lines for a paired loop-like magnetic configuration with attracting force (run 2a). The dashed lines at $t = 0$ designate the convection zone. The square box drawn at the base is a part of the base domain and not the whole base domain.

Fig. 5: Temporal evolution of the magnetic field lines for a paired arcade-like magnetic configuration with attracting force (run 2c). The dashed lines at $t = 0$ designate the convection zone. The square box drawn at the base is a part of the base domain and not the whole base domain.

Fig. 6: Temporal evolution of the magnetic field lines for a paired arcade-like magnetic configuration with repulsive force (run 2c'). The dashed lines at $t = 0$

designate the convection zone.

Fig. 7: Plasma flows on the $x - z$ plane at $t = 6\tau_A$ for the case of paired arcade-like magnetic configuration (run 2c).

Fig. 8: Comparison of the evolutions of the ohmic, viscous and total heating rates with the attractive (a) and repulsive (b) forces for a paired arcade-like configuration.

Fig. 9: The dashed line represents the temporal evolution of the difference between the magnetic energies with the repulsive and attractive forces for a paired arcade-like configuration. The solid line represents the temporal evolution of its time derivative.

Fig. 10: Comparison of the evolutions of the ohmic, viscous and total heating rates for the low resistivity (a: $\eta = 10^{-4}$) and high resistivity (b: $\eta = 10^{-3}$) cases.

Table 1(a): Parameters of simulation runs for a single loop/arcade

case	r_x	r_y	v_0	T_s	r_{10}	r_{20}
1a	$L_x/32$	$L_x/32$	0.1	2	2/3	1
1b	$L_x/32$	$5L_x/32$	0.1	2	2/3	1
1c	$L_x/32$	$15L_x/32$	0.1	2	2/3	1

Table 1(b): Parameters of simulation runs for a paired loop/arcade

case	r_x	r_y	v_0	T_s	r_{10}	r_{20}	polarity of B_0	direction of rotation
2a	$L_x/32$	$L_x/32$	0.1	2	2/3	1	$-+-+$	$++--$
2b	$5L_x/32$	$L_x/32$	0.1	2	2/3	1	$-+-+$	$++--$
2c	$15L_x/32$	$L_x/32$	0.1	2	2/3	1	$-+-+$	$++--$
2c'	$15L_x/32$	$L_x/32$	0.1	2	2/3	1	$-+-+$	$++++$
2c"	$15L_x/32$	$L_x/32$	0.2	2	2/3	1	$-+-+$	$++--$

where +(-) indicates counterclockwise(clockwise) motion in the top view in the item of direction of motion.

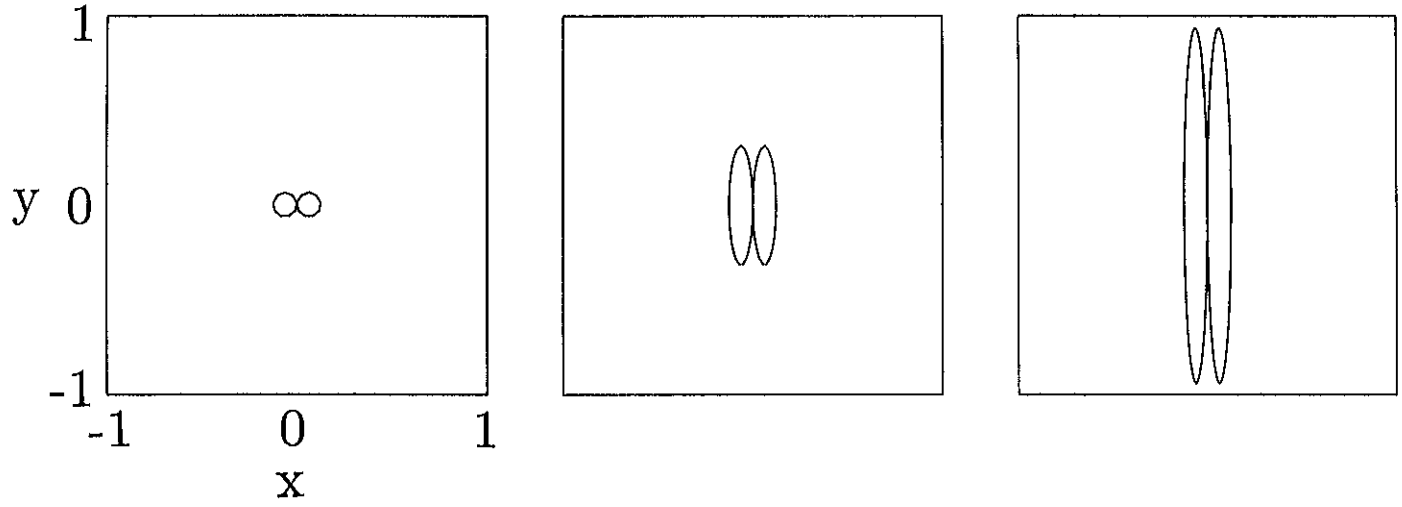

(a) 1a (b) 1b (c) 1c

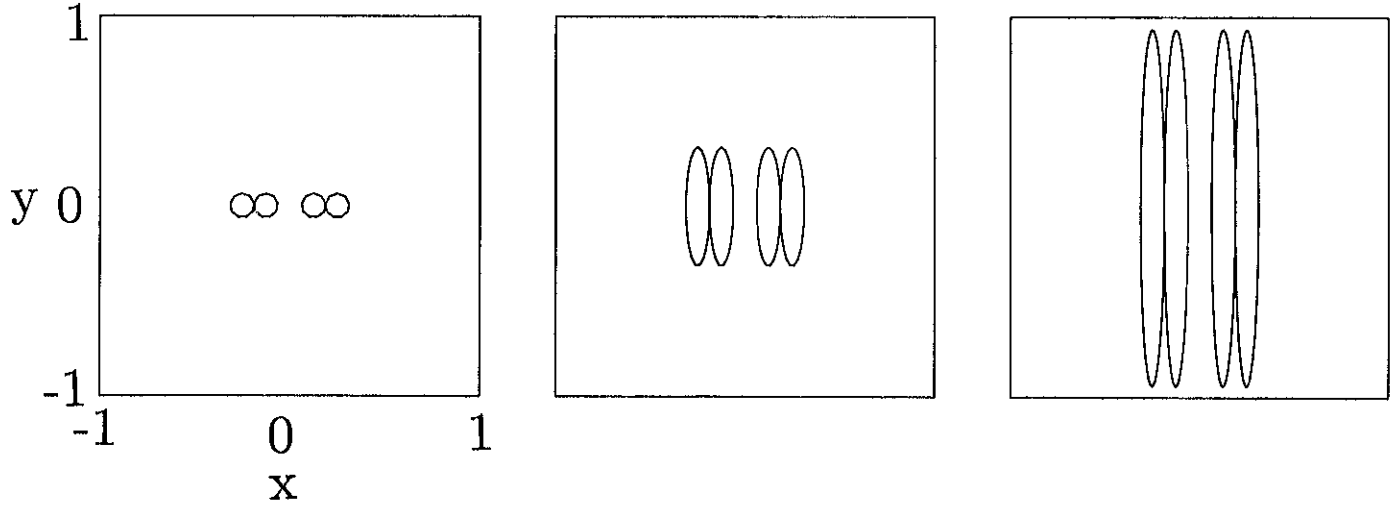

(d) 2a (e) 2b (f) 2c

Fig. 1

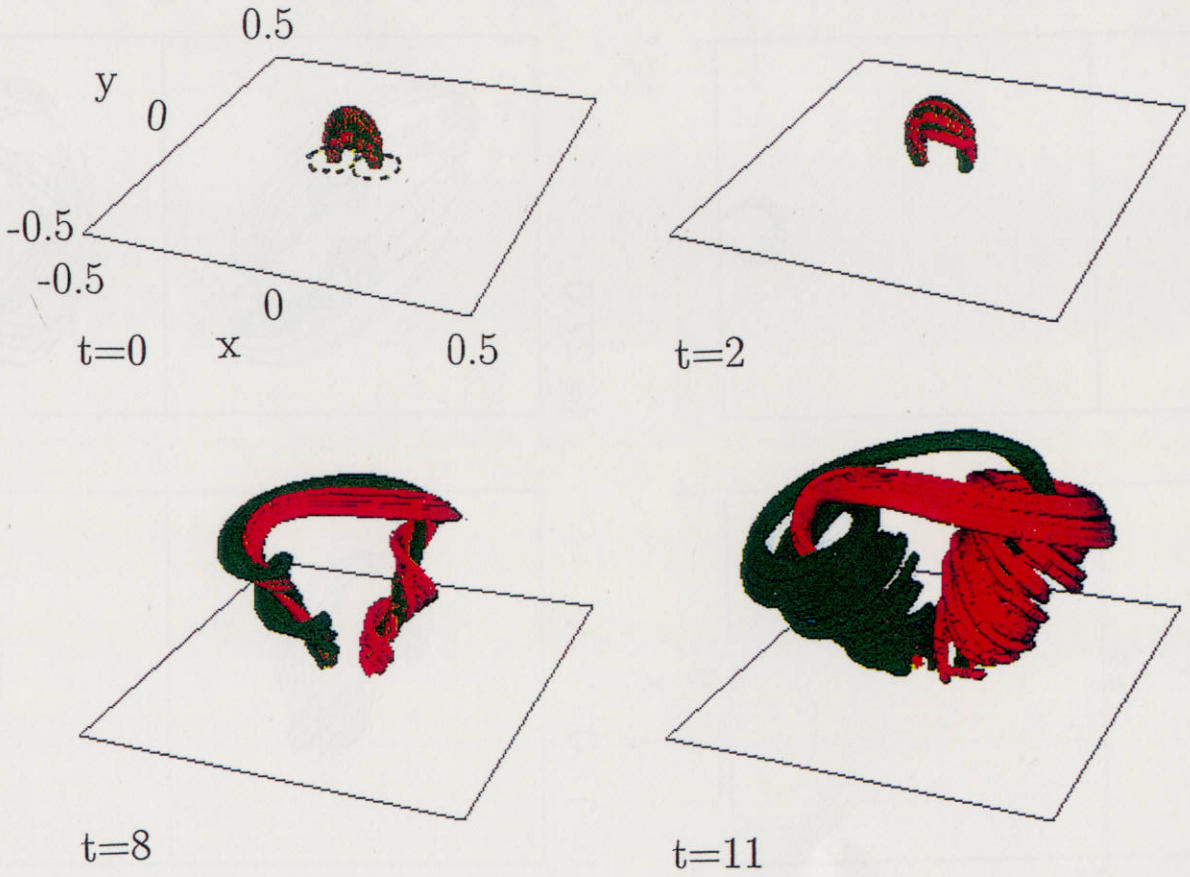

Fig. 2

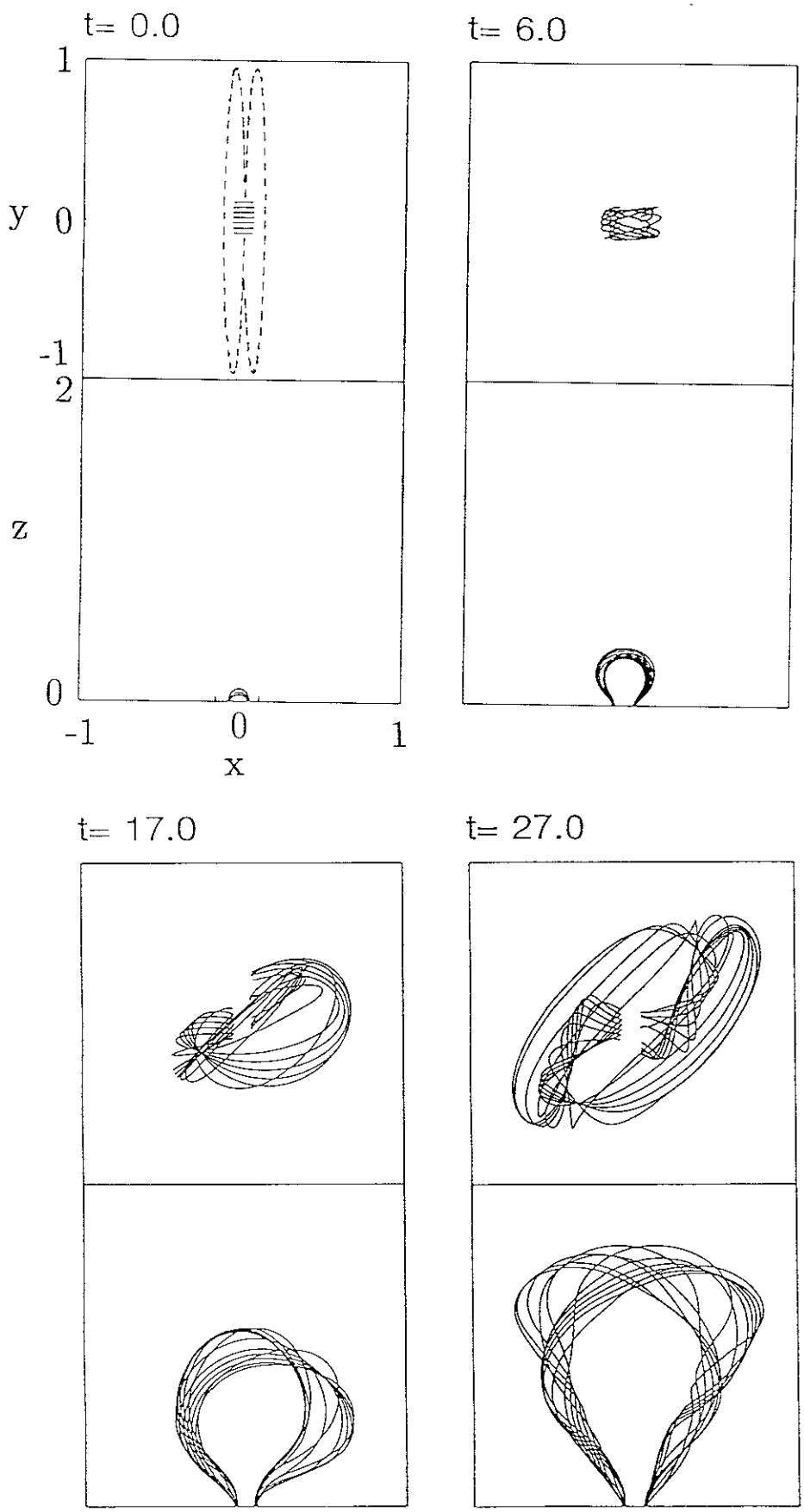

Fig. 3

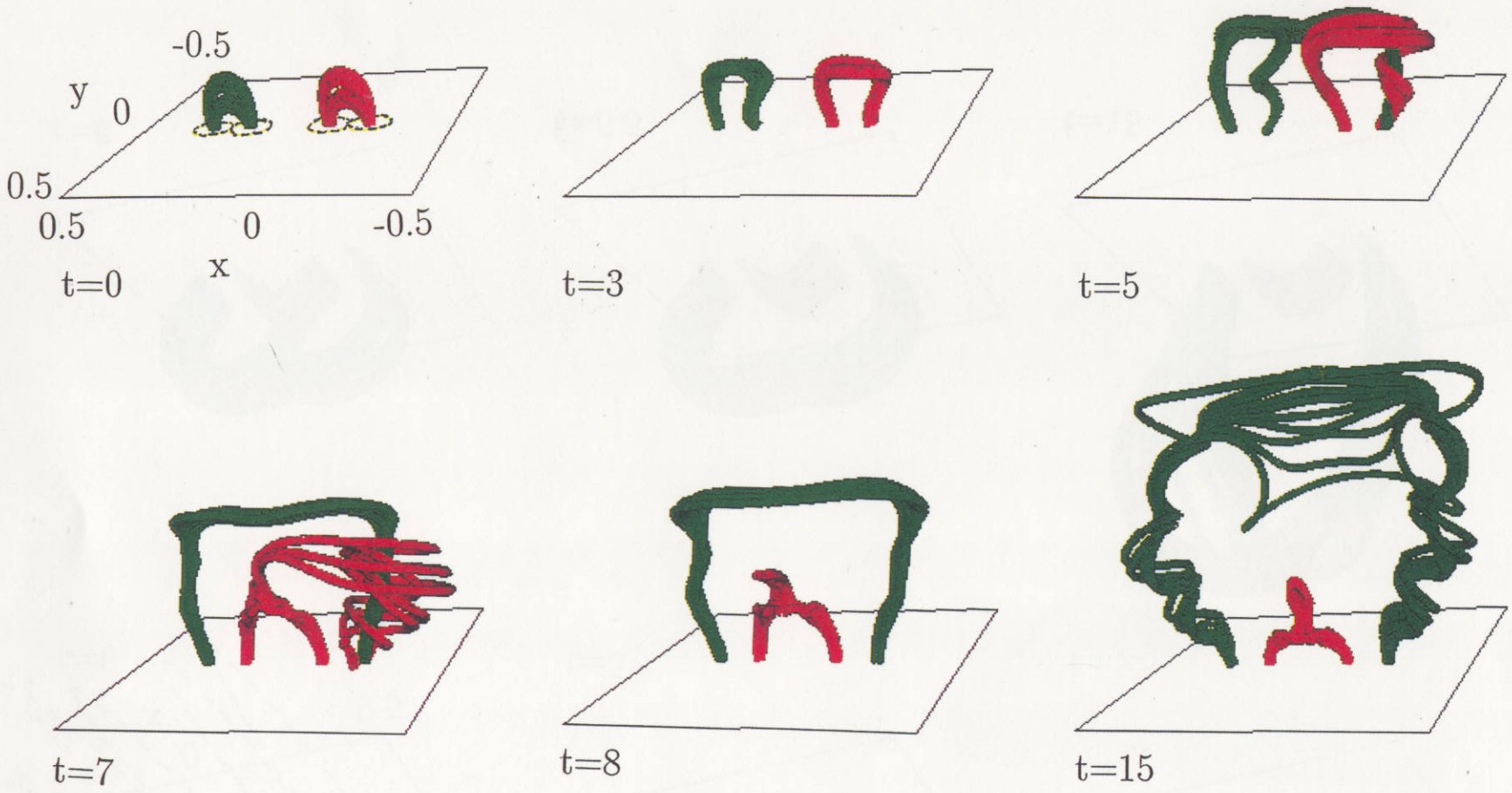

Fig. 4

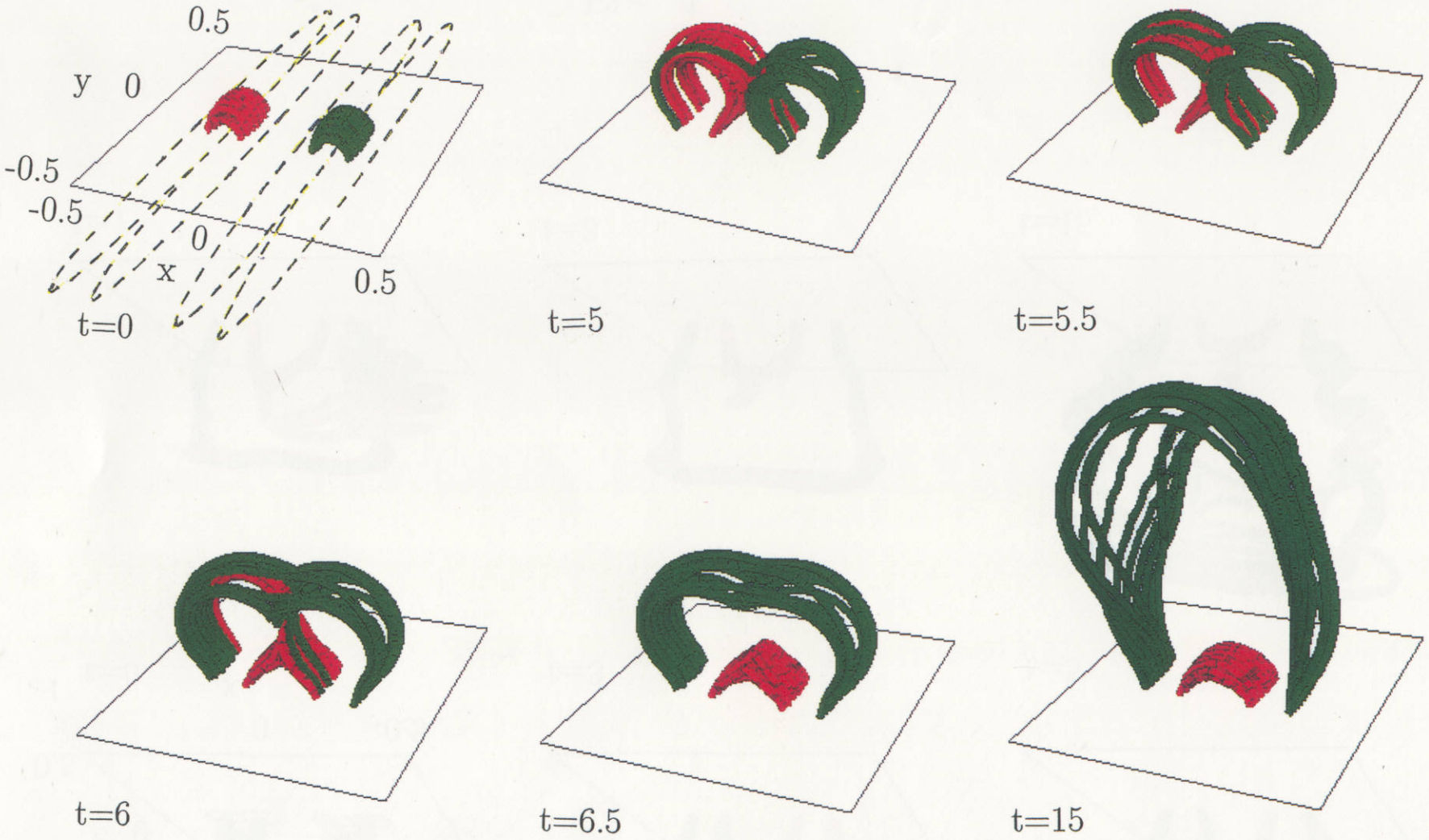

Fig. 5

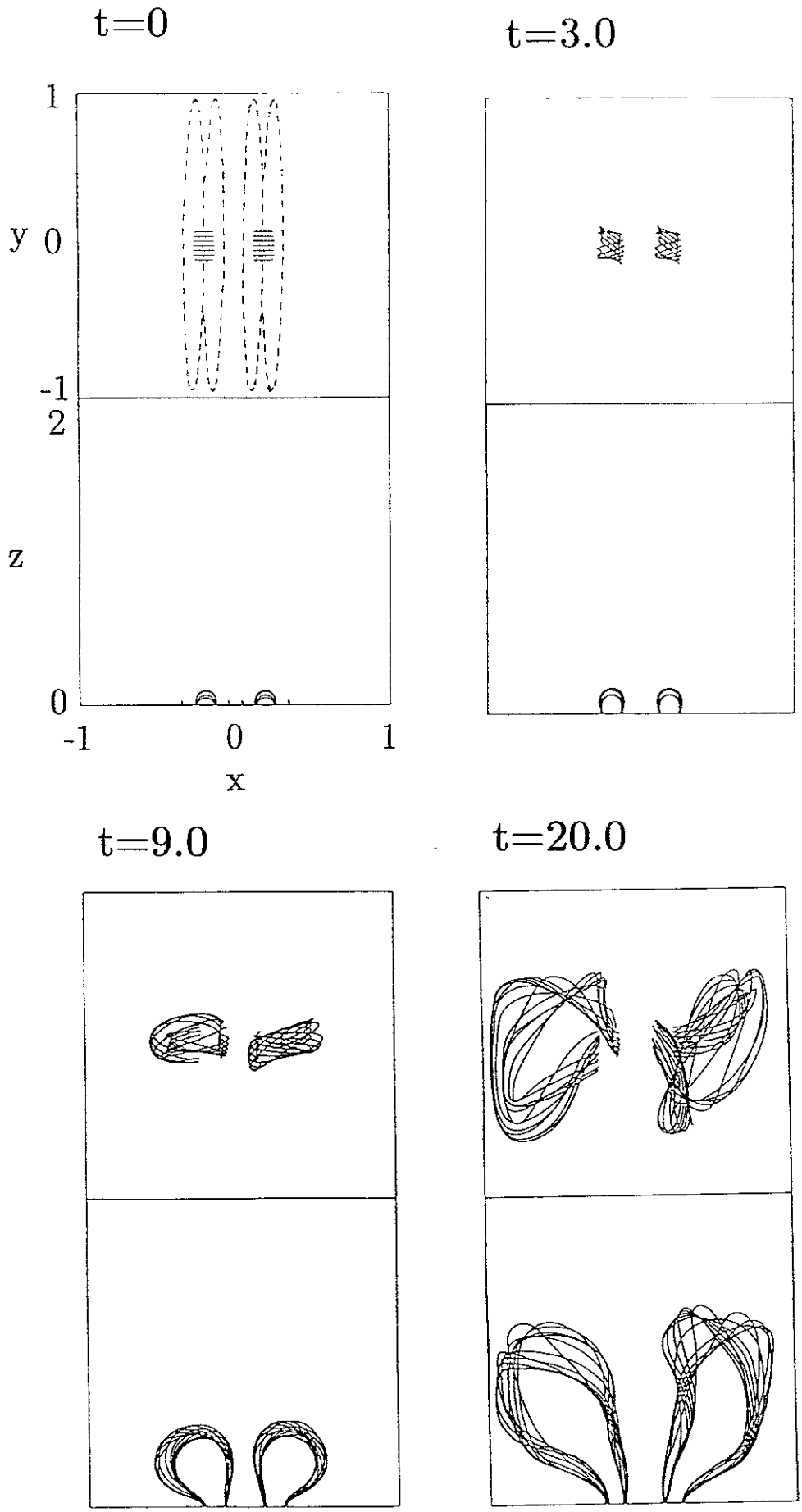

Fig. 6

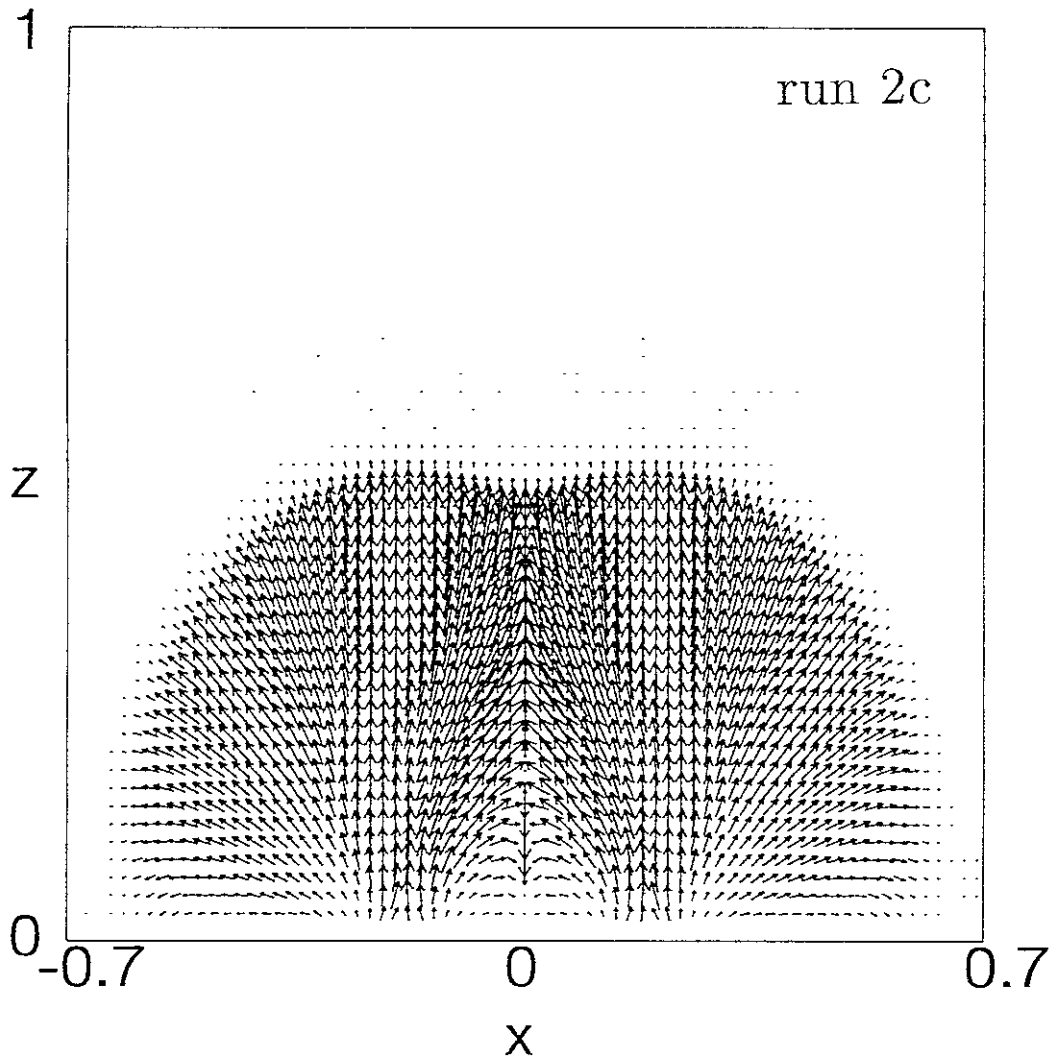

Fig. 7

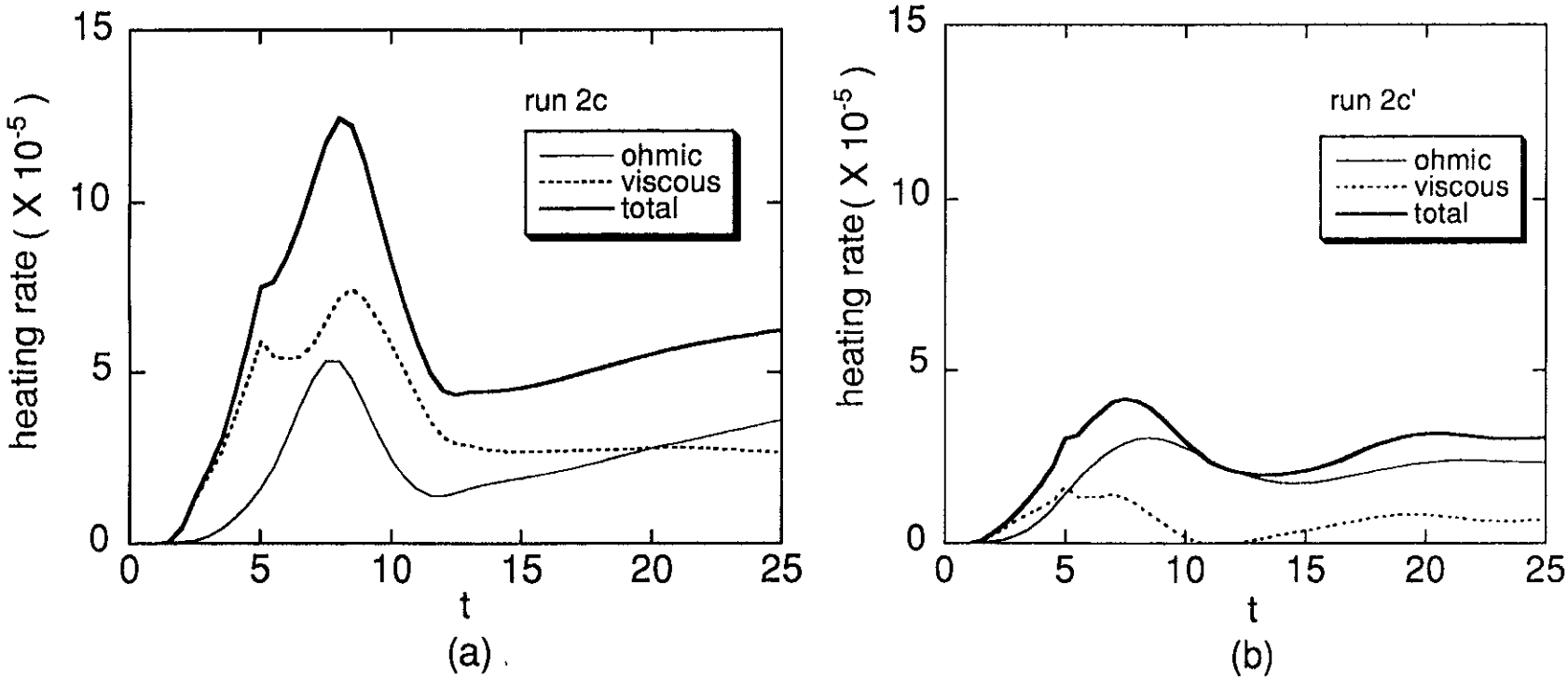
heating rate (X 10^-5)
run 2c
ohmic
viscous
total
t
(a)
heating rate (X 10^-5)
run 2c'
ohmic
viscous
total
t
(b)

Fig. 8

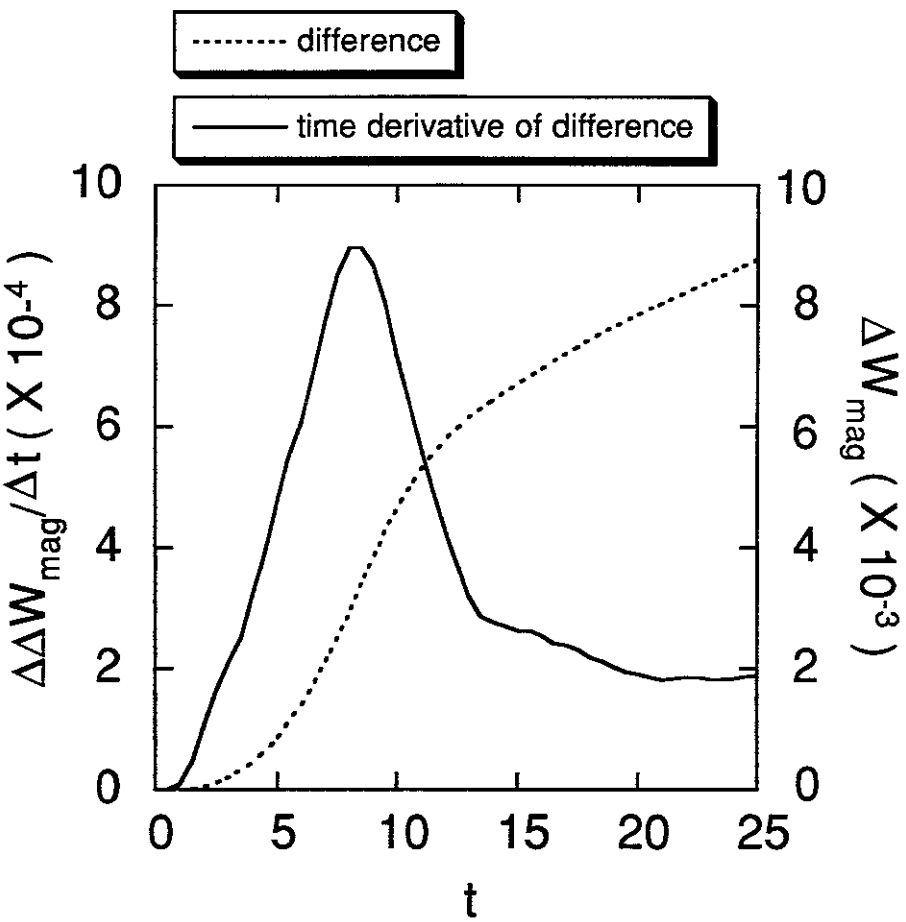
difference
time derivative of difference
10
8
6
4
2
0
0
5
10
15
20
25
t
ΔΔW_mag/Δt (X 10^-4)
ΔW_mag (X 10^-3)

Fig. 9

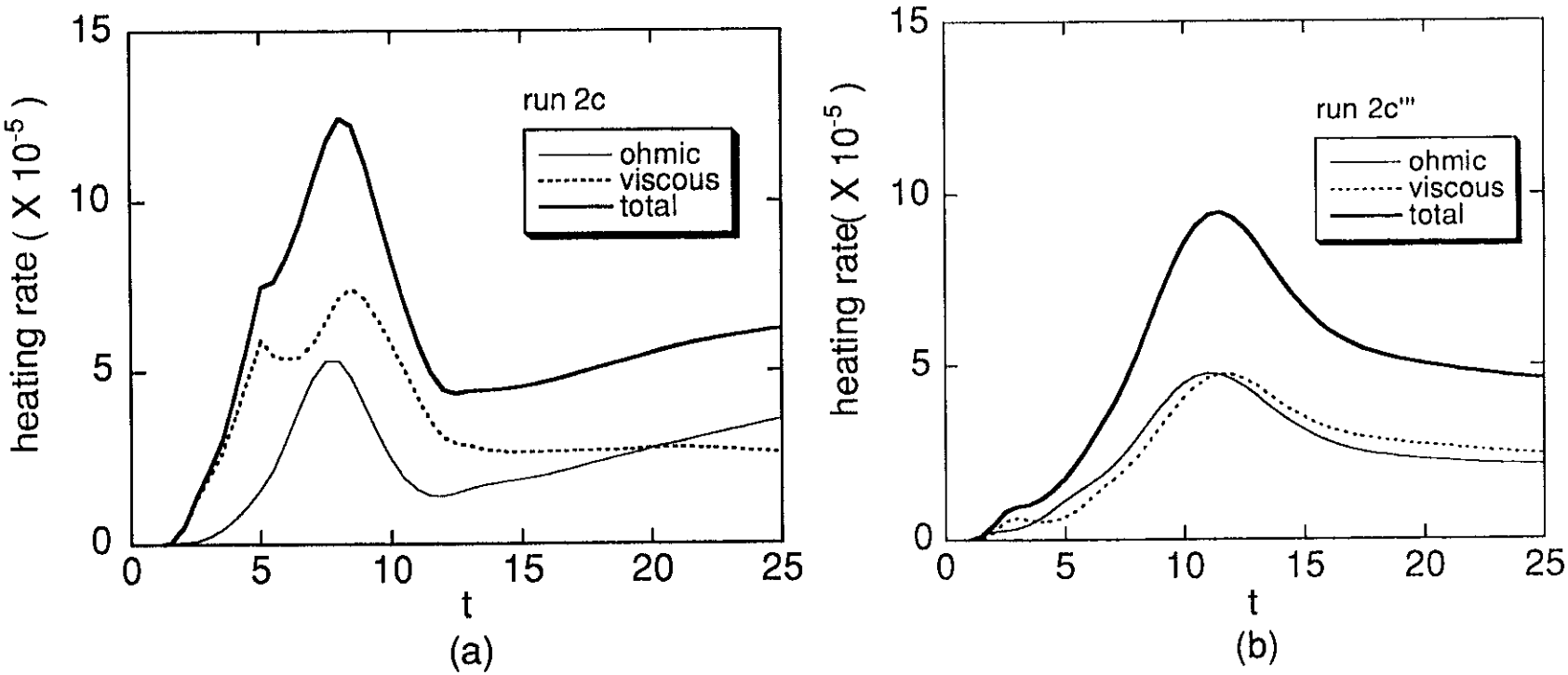
heating rate (X 10^-5)
run 2c
ohmic
viscous
total
t
(a)
heating rate(X 10^-5)
run 2c'''
ohmic
viscous
total
t
(b)

Fig. 10

Recent Issues of NIFS Series

NIFS-412 T. Ohkawa and H. Ohkawa,
Cuspher, A Combined Confinement System; Apr. 1996

NIFS-413 Y. Nomura, Y.H. Ichikawa and A.T. Filippov,
Stochasticity in the Josephson Map; Apr. 1996

NIFS-414 J. Uramoto,
Production Mechanism of Negative Pionlike Particles in H_2 Gas Discharge Plasma; Apr. 1996

NIFS-415 A. Fujisawa, H. Iguchi, S. Lee, T.P. Crowley, Y. Hamada, S. Hidekuma, M. Kojima,
Active Trajectory Control for a Heavy Ion Beam Probe on the Compact Helical System; May 1996

NIFS-416 M. Iwase, K. Ohkubo, S. Kubo and H. Idei
Band Rejection Filter for Measurement of Electron Cyclotron Emission during Electron Cyclotron Heating; May 1996

NIFS-417 T. Yabe, H. Daido,T. Aoki, E. Matsunaga and K. Arisawa,
Anomalous Crater Formation in Pulsed-Laser-Illuminated Aluminum Slab and Debris Distribution; May 1996

NIFS-418 J. Uramoto,
Extraction of K^- Mesonlike Particles from a D_2 Gas Discharge Plasma in Magnetic Field; May 1996

NIFS-419 J. Xu, K. Toi, H. Kuramoto, A. Nishizawa, J. Fujita, A. Ejiri, K. Narihara, T. Seki, H. Sakakita, K. Kawahata, K. Ida, K. Adachi, R. Akiyama, Y. Hamada, S. Hirokura, Y. Kawasumi, M. Kojima, I. Nomura, S. Ohdachi, K.N. Sato
Measurement of Internal Magnetic Field with Motional Stark Polarimetry in Current Ramp-Up Experiments of JIPP T-IIU; June 1996

NIFS-420 Y.N. Nejoh,
Arbitrary Amplitude Ion-acoustic Waves in a Relativistic Electron-beam Plasma System; July 1996

NIFS-421 K. Kondo, K. Ida, C. Christou, V.Yu.Sergeev, K.V.Khlopenkov, S.Sudo, F. Sano, H. Zushi, T. Mizuuchi, S. Besshou, H. Okada, K. Nagasaki, K. Sakamoto, Y. Kurimoto, H. Funaba, T. Hamada, T. Kinoshita, S. Kado, Y. Kanda, T. Okamoto, M. Wakatani and T. Obiki,
Behavior of Pellet Injected Li Ions into Heliotron E Plasmas; July 1996

NIFS-422 Y. Kondoh, M. Yamaguchi and K. Yokozuka,
Simulations of Toroidal Current Drive without External Magnetic Helicity Injection; July 1996

NIFS-423 Joong-San Koog,
Development of an Imaging VUV Monochromator in Normal Incidence Region: July 1996

NIFS-424 K. Orito,
A New Technique Based on the Transformation of Variables for Nonlinear Drift and Rossby Vortices; July 1996

NIFS-425 A. Fujisawa, H. Iguchi, S. Lee, T.P. Crowley, Y. Hamada, H. Sanuki, K. Itoh, S. Kubo, H. Idei, T. Minami, K. Tanaka, K. Ida, S. Nishimura, S. Hidekuma, M. Kojima, C. Takahashi, S. Okamura and K. Matsuoka,
Direct Observation of Potential Profiles with a 200keV Heavy Ion Beam Probe and Evaluation of Loss Cone Structure in Toroidal Helical Plasmas on the Compact Helical System; July 1996

NIFS-426 H. Kitauchi, K. Araki and S. Kida,
Flow Structure of Thermal Convection in a Rotating Spherical Shell; July 1996

NIFS-427 S. Kida and S. Goto,
Lagrangian Direct-interaction Approximation for Homogeneous Isotropic Turbulence; July 1996

NIFS-428 V.Yu. Sergeev, K.V. Khlopenkov, B.V. Kuteev, S. Sudo, K. Kondo, F. Sano, H. Zushi, H. Okada, S. Besshou, T. Mizuuchi, K. Nagasaki, Y. Kurimoto and T. Obiki,
Recent Experiments on Li Pellet Injection into Heliotron E; Aug. 1996

NIFS-429 N. Noda, V. Philipps and R. Neu,
A Review of Recent Experiments on W and High Z Materials as Plasma-Facing Components in Magnetic Fusion Devices; Aug. 1996

NIFS-430 R.L. Tobler, A. Nishimura and J. Yamamoto,
Design-Relevant Mechanical Properties of 316-Type Stainless Steels for Superconducting Magnets; Aug. 1996

NIFS-431 K. Tsuzuki, M. Natsir, N. Inoue, A. Sagara, N. Noda, O. Motojima, T. Mochizuki, T. Hino and T. Yamashina,
Hydrogen Absorption Behavior into Boron Films by Glow Discharges in Hydrogen and Helium; Aug. 1996

NIFS-432 T.-H. Watanabe, T. Sato and T. Hayashi,
Magnetohydrodynamic Simulation on Co- and Counter-helicity Merging of Spheromaks and Driven Magnetic Reconnection; Aug. 1996

NIFS-433 R. Horiuchi and T. Sato,
Particle Simulation Study of Collisionless Driven Reconnection in a Sheared

Magnetic Field; Aug. 1996

NIFS-434 Y. Suzuki, K. Kusano and K. Nishikawa.
Three-Dimensional Simulation Study of the Magnetohydrodynamic Relaxation Process in the Solar Corona. II., Aug. 1996

NIFS-435 H. Sugama and W. Horton,
Transport Processes and Entropy Production in Toroidally Rotating Plasmas with Electrostatic Turbulence; Aug. 1996

NIFS-436 T. Kato, E. Rachlew-Källne, P. Hörling and K.-D Zastrow,
Observations and Modelling of Line Intensity Ratios of OV Multiplet Lines for 2s3s 3S1 - 2s3p 3Pj; Aug. 1996

NIFS-437 T. Morisaki, A. Komori, R. Akiyama, H. Idei, H. Iguchi, N. Inoue, Y. Kawai, S. Kubo, S. Masuzaki, K. Matsuoka, T. Minami, S. Morita, N. Noda, N. Ohyabu, S. Okamura, M. Osakabe, H. Suzuki, K. Tanaka, C. Takahashi, H. Yamada, I. Yamada and O. Motojima,
Experimental Study of Edge Plasma Structure in Various Discharges on Compact Helical System; Aug. 1996

NIFS-438 A. Komori, N. Ohyabu, S. Masuzaki, T. Morisaki, H. Suzuki, C. Takahashi, S. Sakakibara, K. Watanabe, T. Watanabe, T. Minami, S. Morita, K. Tanaka, S. Ohdachi, S. Kubo, N. Inoue, H. Yamada, K. Nishimura, S. Okamura, K. Matsuoka, O. Motojima, M. Fujiwara, A. Iiyoshi, C. C. Klepper, J.F. Lyon, A.C. England, D.E. Greenwood, D.K. Lee, D.R. Overbey, J.A. Rome, D.E. Schechter and C.T. Wilson,
Edge Plasma Control by a Local Island Divertor in the Compact Helical System; Sep. 1996 (IAEA-CN-64/C1-2)

NIFS-439 K. Ida, K. Kondo, K. Nagaski T. Hamada, H. Zushi, S. Hidekuma, F. Sano, T. Mizuuchi, H. Okada, S. Besshou, H. Funaba, Y. Kurimoto, K. Watanabe and T. Obiki,
Dynamics of Ion Temperature in Heliotron-E; Sep. 1996 (IAEA-CN-64/CP-5)

NIFS-440 S. Morita, H. Idei, H. Iguchi, S. Kubo, K. Matsuoka, T. Minami, S. Okamura, T. Ozaki, K. Tanaka, K. Toi, R. Akiyama, A. Ejiri, A. Fujisawa, M. Fujiwara, M. Goto, K. Ida, N. Inoue, A. Komori, R. Kumazawa, S. Masuzaki, T. Morisaki, S. Muto, K. Narihara, K. Nishimura, I. Nomura, S. Ohdachi, M.. Osakabe, A. Sagara, Y. Shirai, H. Suzuki, C. Takahashi, K. Tsumori, T. Watari, H. Yamada and I. Yamada,
A Study on Density Profile and Density Limit of NBI Plasmas in CHS; Sep. 1996 (IAEA-CN-64/CP-3)

NIFS-441 O. Kaneko, Y. Takeiri, K. Tsumori, Y. Oka, M. Osakabe, R. Akiyama, T. Kawamoto, E. Asano and T. Kuroda,
Development of Negative-Ion-Based Neutral Beam Injector for the Large Helical Device; Sep. 1996 (IAEA-CN-64/GP-9)

NIFS-442 K. Toi, K.N. Sato, Y. Hamada, S. Ohdachi, H. Sakakita, A. Nishizawa, A. Ejiri, K. Narihara, H. Kuramoto, Y. Kawasumi, S. Kubo, T. Seki, K. Kitachi, J. Xu, K. Ida, K. Kawahata, I. Nomura, K. Adachi, R. Akiyama, A. Fujisawa, J. Fujita, N. Hiraki, S. Hidekuma, S. Hirokura, H. Idei, T. Ido, H. Iguchi, K. Iwasaki, M. Isobe, O. Kaneko, Y. Kano, M. Kojima, J. Koog, R. Kumazawa, T. Kuroda, J. Li, R. Liang, T. Minami, S. Morita, K. Ohkubo, Y. Oka, S. Okajima, M. Osakabe, Y. Sakawa, M. Sasao, K. Sato, T. Shimpo, T. Shoji, H. Sugai, T. Watari, I. Yamada and K. Yamauti,
Studies of Perturbative Plasma Transport, Ice Pellet Ablation and Sawtooth Phenomena in the JIPP T-IIU Tokamak; Sep. 1996 (IAEA-CN-64/A6-5)

NIFS-443 Y. Todo, T. Sato and The Complexity Simulation Group,
Vlasov-MHD and Particle-MHD Simulations of the Toroidal Alfvén Eigenmode; Sep. 1996 (IAEA-CN-64/D2-3)

NIFS-444 A. Fujisawa, S. Kubo, H. Iguchi, H. Idei, T. Minami, H. Sanuki, K. Itoh, S. Okamura, K. Matsuoka, K. Tanaka, S. Lee, M. Kojima, T.P. Crowley, Y. Hamada, M. Iwase, H. Nagasaki, H. Suzuki, N. Inoue, R. Akiyama, M. Osakabe, S. Morita, C. Takahashi, S. Muto, A. Ejiri, K. Ida, S. Nishimura, K. Narihara, I. Yamada, K. Toi, S. Ohdachi, T. Ozaki, A. Komori, K. Nishimura, S. Hidekuma, K. Ohkubo, D.A. Rasmussen, J.B. Wilgen, M. Murakami, T. Watari and M. Fujiwara,
An Experimental Study of Plasma Confinement and Heating Efficiency through the Potential Profile Measurements with a Heavy Ion Beam Probe in the Compact Helical System; Sep. 1996 (IAEA-CN-64/C1-5)

NIFS-445 O. Motojima, N. Yanagi, S. Imagawa, K. Takahata, S. Yamada, A. Iwamoto, H. Chikaraishi, S. Kitagawa, R. Maekawa, S. Masuzaki, T. Mito, T. Morisaki, A. Nishimura, S. Sakakibara, S. Satoh, T. Satow, H. Tamura, S. Tanahashi, K. Watanabe, S. Yamaguchi, J. Yamamoto, M.Fujiwara and A. Iiyoshi,
Superconducting Magnet Design and Construction of LHD; Sep. 1996 (IAEA-CN-64/G2-4)

NIFS-446 S. Murakami, N. Nakajima, S. Okamura, M. Okamoto and U. Gasparino,
Orbit Effects of Energetic Particles on the Reachable β–Value and the Radial Electric Field in NBI and ECR Heated Heliotron Plasmas; Sep. 1996 (IAEA-CN-64/CP -6) Sep. 1996

NIFS-447 K. Yamazaki, A. Sagara, O. Motojima, M. Fujiwara, T. Amano, H. Chikaraishi, S. Imagawa, T. Muroga, N. Noda, N. Ohyabu, T. Satow, J.F. Wang, K.Y. Watanabe, J. Yamamoto , H. Yamanishi, A. Kohyama, H. Matsui, O. Mitarai, T. Noda, A.A. Shishkin, S. Tanaka and T. Terai
Design Assessment of Heliotron Reactor; Sep. 1996 (IAEA-CN-64/G1-5)

NIFS-448 M. Ozaki, T. Sato and the Complexity Simulation Group,
Interactions of Convecting Magnetic Loops and Arcades; Sep. 1996